Tribology International 118 (2018) 474–483

Contents lists available at ScienceDirect

Tribology International

journal homepage: www.elsevier.com/locate/triboint

Mechanical characterization and single asperity scratch behaviour of dry zinc and manganese phosphate coatings

D. Ernens [a,b,*], M.B. de Rooij [a], H.R. Pasaribu [b], E.J. van Riet [b], W.M. van Haaften [b], D.J. Schipper [a]

[a] Laboratory for Surface Technology and Tribology, Department of Engineering Technology, University of Twente, P.O. Box 217, 7500 AE Enschede, The Netherlands
[b] Shell Global Solutions International BV, Innovation, Research & Development, Wells R & D, Kessler Park 1, 2288 GS Rijswijk, The Netherlands

ARTICLE INFO

Keywords:
Mechanical characterization
Phosphate conversion coatings
Scratch test
Nano-indentation

MSC:
00-01
99-00

ABSTRACT

The goal of this study is to characterise the mechanical properties of zinc and manganese phosphate coatings before and after running in. The characterization is done with nano-indentation to determine the individual crystal hardness and single asperity scratch tests to investigate the deformation behaviour at the single asperity level. The nano-indentation and scratch tests reveal brittle deformation behaviour for the as received coatings. Under uni-directional sliding both layers reduce to a powder which is subsequently compacted to a so called glaze layer. The smooth and brittle glaze layer has a higher hardness compared to the as received coating and its properties can be satisfactorily described by models normally used for a hard coating on a soft substrate.

1. Introduction

Phosphate conversion coatings are often used to facilitate the running-in phase of machine elements [1]. In the oil and gas industry these coatings are, amongst others, used as corrosion protection [2–5] of casing connections during storage. An added benefit of the coatings is the improved galling resistance in the assembly phase [6].

The casing connections contain a metal-to-metal seal to ensure pressure integrity of the created conduit after installation. The sealing performance of metal-to-metal seals has been shown to be determined by the surface texture and changes thereof [7–10]. Phosphate coatings, therefore, play an important role in the seal ability of the casing connections.

Typically zinc and manganese coatings consist of respectively hopeite [11] and hureaulite [12] crystals. The crystal hardness is reported by [13] to be 3.2 and 5 on the Mohs scale. Others report 2.5–3 Mohs and 3.5 Mohs respectively [1]. As the Mohs scale is ordinal, this only says that hureaulite is harder than hopeite. The equivalent Vickers hardness is 102–229 HV.

Kumar et al. [14] characterized zinc phosphate using micro hardness indentations, wear experiments and corrosion experiments. They determined the micro hardness of the layer to be 50 HV and found that the needle structure of zinc phosphate crystals plays an important role in the wear behaviour of medium alloy low carbon steel. The experimentally observed wear increase was attributed to the roughening of the surface and the subsequent increase in local contact stress. They found that the phosphate process introduces considerable compressive residual stresses in the substrate reducing fretting resistance. Furthermore, they observed an increase in the coefficient of friction (COF) compared to bare steel attributed to the increased contact area due to the softer layer. Finally, they concluded that zinc phosphate is not effective in increasing wear resistance.

The authors of this paper attribute the introduction of compressive stresses to epitaxy. In [1] a misfit of -7% between the hopeite lattice and α-Fe lattice is reported which indeed leads to tensile stresses in the coating and thus compressive stresses in the substrate. Interestingly the misfit of hureaulite is -1% and should thus lead to less issues with wear resistance of the coating.

Previous work on the mechanical characterization of manganese phosphate coatings was conducted by [15]. They derived a bulk behaviour law for manganese phosphate based on micro hardness indentations combined with a finite element model. The finite element analysis is used to match the experimental indentation data to provide the stress – strain curves assuming a non-layered material. The combined data is fitted to a modified Ludwick model. The procedure yields a continuous material model that incorporates the coating to bulk transition. The surface hardness was measured to be 125 HV.

The wear characteristics as function of the applied phosphating process were first investigated by [3]. The findings were that a thin fine

* Corresponding author at: Laboratory for Surface Technology and Tribology, Department of Engineering Technology, University of Twente, P.O. Box 217, 7500 AE Enschede, The Netherlands.
E-mail address: d.ernens@utwente.nl (D. Ernens).

https://doi.org/10.1016/j.triboint.2017.04.034
Received 20 September 2016; Received in revised form 19 April 2017; Accepted 21 April 2017
Available online 25 April 2017
0301-679X/

grained coating gives superior wear performance. A more elaborate study on the relation between the coating process and the seizure behaviour of manganese phosphate was done by [16]. Considerable improvements were obtained by fine tuning the cleaning, refining and phosphating parameters. They also showed that the carbon content of the substrate plays a significant role. Next to that they found that annealing the coating yields considerable improvements in seizure resistance related to improved oil retaining properties and increased surface hardness from 125 HV to 300 HV [17,15].

The general conclusion for the previous research was that the COF goes down with increasing load and repeated sliding. This is attributed to the formation of a flat and smooth glaze layer after sustained sliding [1]. It is also suggested in [13,1] that the phosphate layers have a certain directionality or anisotropy owing to the crystal growth and aforementioned epitaxy leading to slight differences in deformation behaviour.

The cited investigators focused on long running systems and characterization of the friction and wear at the macroscopic level. However, the metal-to-metal seal undergoes a maximum total sliding length of <0.5 m during assembly [18]. Short running systems, like casing connections, and the deformation mechanism at the asperity level that gives rise to the macroscopic friction and wear observations have not been investigated. In order to properly model the phosphate coatings in a contact and wear model [19] to predict its influence on seal ability a characterization of their properties needs to be performed. This study aims to characterize the deformation mechanism(s) of the phosphate coatings before and after formation of a glaze layer.

2. Methods

In order to obtain fundamental insight in the effect of phosphate coatings on surface evolution and thus sealing performance it is important to characterise the initial phosphate layer as well as the evolution of the phosphate layer. For the deformation behaviour nano-indentation and scratch experiments are performed. The wear mode is determined according to the works of [20,21]. The scratch tests will also be used to determine layer hardness and shear strength using the method introduced by Tayebi, Conry and Polycarpou (TCP) [22].

2.1. Phosphated specimens

The phosphated specimens were prepared from quenched and tempered AISI4130 steel by water jetting 70×70×2 mm coupons from 100 mm bar material. These were subsequently ground on both sides to a surface finish of $R_a = 0.1$ μm. The substrate hardness was measured prior to phosphating by the method of Section 2.3 at 500 mN resulting in a hardness of 1.96±0.3 GPa.

After grinding, the specimens were cleaned, degreased and water rinsed before they were dipped in the zinc or manganese phosphate bath. See Table 1 for an overview of the process parameters. The resulting coating weights are reported in the final row. Note, however, that due to the morphology a coating thickness is difficult to define [1]. Therefore absolute depths are reported in the results.

Table 1
Overview of the phosphate conversion coating process for the AISI4130 substrate.

Step	Treatment	Zinc phosphate	Manganese phosphate
1	Degreasing	Gardoclean® 349, 50 g/l, 75 °C, 10 min dip	
2	Rinsing	cold water	
3	Activation	Gardolene® V6522, 2 g/l, 40 °C, 1 min dip	Gardolene® V6563, 4 g/l, 40 °C, 1 min dip
4	Phosphating	Gardobond® Z3300, 75 °C, 5 min dip time, Free acid: 18, Total acid: 112, Fe++: 0.9 g/l	Gardobond® G4098+5 g/l Gardobond®Additive H7050, 90 °C, 5 min dip time, Free acid: 18; Total acid: 119; Fe++: 1 g/l
5	Rinsing	cold water & demineralized water	
6	Drying	oven 95 °C	
–	Coating weight	4.5 g/m^2	10.95 g/m^2

SEM micrographs of the coating are shown in Fig. 2. The morphology for the zinc phosphate is the distinct needle shape [1] in agreement with its orthorombic dipyramidal unit cell [11]. The morphology for manganese phosphate is the characteristic plate structure [1] coming from its monoclinic prismatic unit cell [12]. The manganese phosphate process produces a much denser and more refined coating compared to zinc phosphate. The surface roughness of the coatings was measured using a confocal microscope (Keyence VK-9700) and is shown in Fig. 1. This shows that zinc phosphate (Fig. 1a) produces a much rougher surface compared to manganese phosphate (Fig. 1b).

X-ray diffraction (XRD) measurements were performed to characterize the phosphate crystal type. The measurements were performed on 2 different positions on the sample surface. For the manganese phosphate coatings, an additional measurement with a measurement time of 3600 s/frame was performed. The measurement settings are reported in Appendix A. The XRD characterization of the specimens confirms that the crystal structure for zinc phosphate is predominantly hopeite [11] while for manganese phosphate it is hureaulite [12], see Fig. 3.

2.2. Experimental design of the scratch experiments

The scratch experiments are designed according to the work of [20]. The relations used to dimension the scratch pins are as follows and assume plastic deformation,

$$\begin{aligned} \theta &= \arctan\sqrt{\frac{h(2r-h)}{r-h}} \\ h_{sliding} &= \frac{F_n}{\pi r H}. \end{aligned} \tag{1}$$

Where θ is the attack angle, h is the penetration depth and $h_{sliding}$ the penetration depth during sliding. Based on Eq. (1) and assuming a constant hardness, H, of 50 HV 0.005 of the coating layer according to [14] two scratch pins with different round off radii were selected.

A sharp indenter made of quenched and tempered Sverker21 steel with a round-off radius, r, of 100 μm which connects in a continuous manner to a 90° conical section [20]. The surface hardness is 700 HV and the surface finish is polished with an $R_a = 0.01$ μm. A ball was used for lower contact angles at higher contact loads and larger contact areas. The ball is made of AISI52100 steel with a radius of 1500 μm, a surface hardness of 700 HV, and a polished surface finish of $R_a = 0.01$ μm. The sliding velocity, v, is chosen as low as possible to minimize thermal effects. Scratch tests with constant load and with increasing load were performed to respectively determine the deformation behaviour, scratch hardness and shear strength of the layers. The tribofilms generated with the ball in the constant load experiments were subsequently used to determined the hardness of the layer and deformation behaviour after run in. The experimental variation is determined by the round-off radius and applied load. The experiments and their resulting attack angle, penetration depth and sliding lengths are summarized in Table 2.

Prior to all the experiments the scratch pins and balls were ultrasonically cleaned in acetone for 15 min, subsequently dried with nitrogen and wiped with lens paper.

The tests were performed on two tribotesters. The ploughing asperity tester [20] and a Bruker UMT-3. The ploughing asperity tester is a dedicated test set-up for single asperity tests. The machine was used for the single unidirectional scratches. The Bruker UMT-3 is a universal mechanical tester which was used in the pin on disc mode. In this case the scratch tracks are placed in an arc. The machine was used for the scratch hardness and the single and repeated unidirectional scratches on a single wear track.

Next to the tribotester (UMT-3) depth measurement, the wear track width and depth are measured using a confocal microscope. The height of

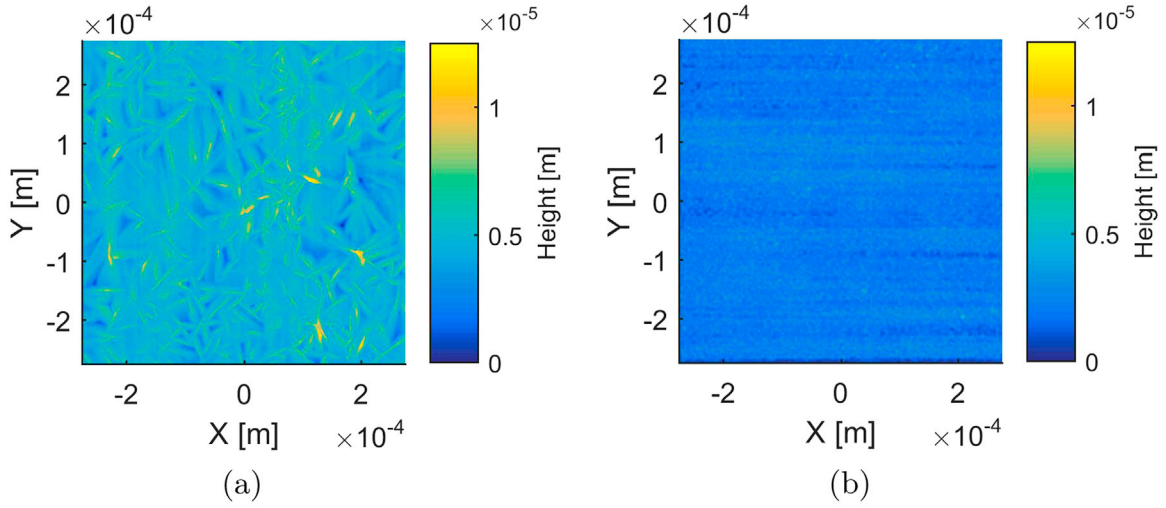

Fig. 1. Height maps using confocal microscopy for both coatings. a) Shows the topology of zinc phosphate and b) for manganese phosphate. Height is scaled to the maximum of zinc phsophate.

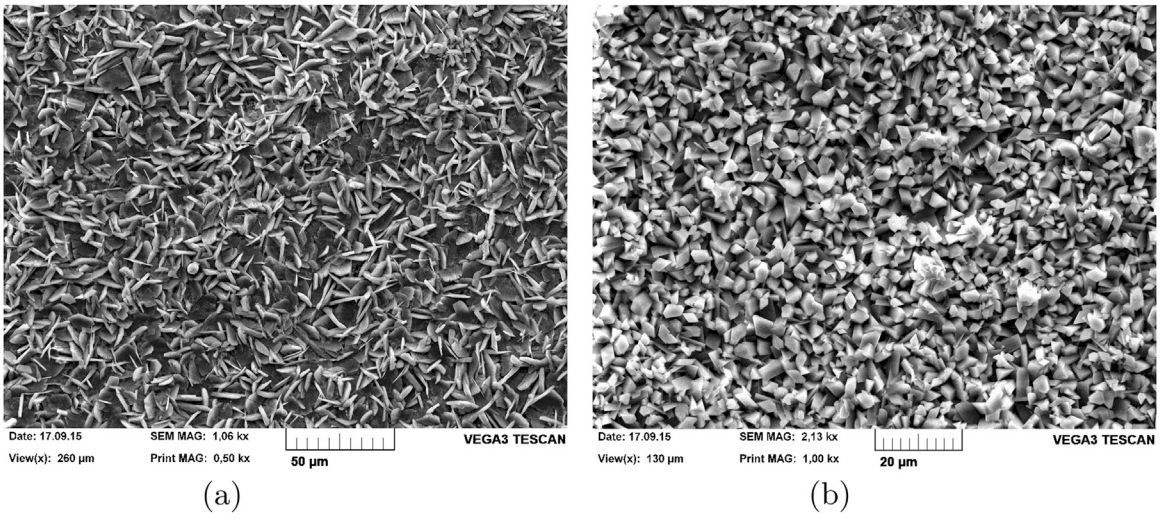

Fig. 2. SEM micrographs of the phosphate coatings and the crystals that they contain. a) Shows zinc phosphate with is characteristic needle structure b) is manganese phosphate with its characteristic plate structure. Note the difference in magnification between the zinc and manganese phosphate specimens.

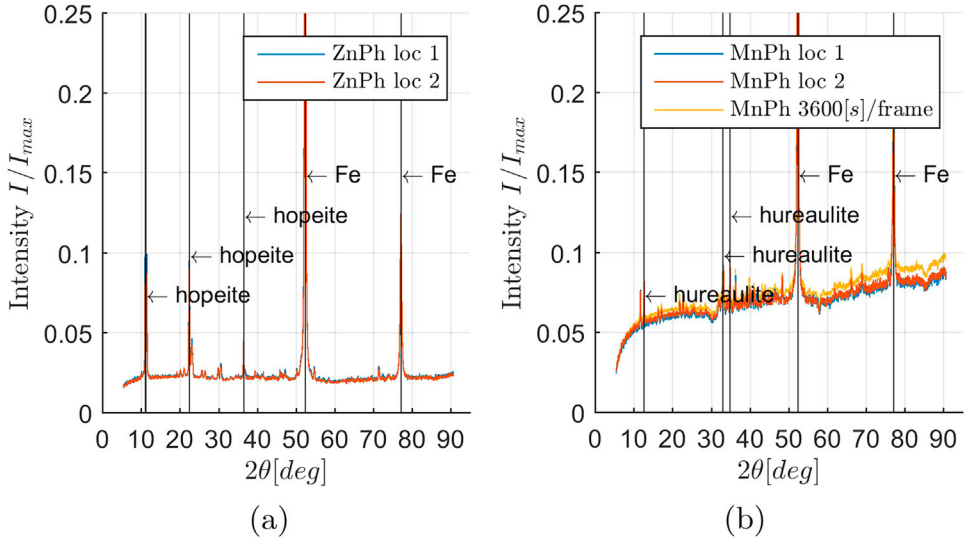

Fig. 3. X-ray diffractogram for zinc and manganese phosphate coated specimens. The intensity is normalized by the maximum intensity. The peaks at 52.4° and 77.3° are from the iron in the substrate. The remaining diffractogram is in agreement with hopeite for zinc phosphate and hureaulite for manganese phosphate. Note that the second XRD measurement for manganese phosphate was performed at 3600 s/frame.

Table 2
Overview of experiments.

Experiment	Passes (#)	r (μm)	F_n (N)	Loading (–)	l (mm)	θ (deg.)	$h_{sliding}$ (μm)	v (mm/s)
Unidirectional	1	100	0.1–5	constant	5	16–45	0.6–32	0.1
	1	1500	5–45	constant	5	3–9	2–20	0.1
	10	1500	5–45	constant	5	3–9	2–20	0.1
Scratch hardness	1	100	0.1–5	ramp	1.8	16–45	0.6–32	0.1

the deposition on the pins is also measured using a confocal microscope. A subset of the pins were inspected using a SEM to identify the deposition using EDX.

2.3. Nano-indentation

Nano-indentation is used to determine the surface hardness of the phosphate coating before and after the generation of the tribofilm or glaze layer [1] in the unidirectional sliding experiments. The goal of the nano-indentation is threefold: to determine the surface hardness of the coatings; to determine the deformation behaviour of the coatings and to determine the transition from coating hardness to substrate hardness as function of penetration depth. These results will then be used to characterize the layers and can serve as input for a layered contact or wear model.

The structure (Fig. 2) of both phosphates gives a rough non-uniform surface (Fig. 1). The indentation results reported here were all placed in the needles for zinc phosphate and in random locations for manganese phosphate. Furthermore, indents were performed in a wear track after 10 passes to investigate how the compaction of the phosphate layers changes the surface hardness and deformation behaviour.

The equipment used for these experiments is the universal nano-mechanical tester (UNAT) built by Asmec. The nano-indentation was carried out using a diamond Berkovich tip. The loads applied ranged from 1 to 500 mN. Each test was repeated 15 times, tests with fracture events were discarded. The load was applied in 10 s, the hold time was 15 s and unloading was performed in 4 s. The tip geometry and measurement set-up were validated prior to the measurements using a sapphire reference. To establish a datum for the indentation tests, an indentation at 0.1 mN is made prior to the measurement. Processing of the force-displacement curves is done according to the method of [23].

2.4. Determination of scratch hardness and shear strength

The hardness and shear strength will be determined from the measured normal, F_n, and tangential force, F_t, with the method of [22], here abbreviated as TPC method, by solving the following system of equations,

$$\begin{aligned} F_t &= Hr^2[\alpha - \sin(\alpha)\cos(\alpha)] + 2sr^2\left[\int_0^{\pi/2}\int_0^{\alpha}\sin(\zeta)\sqrt{\sin^2(\xi)+\cos^2(\xi)\cos^2(\zeta)}\,d\zeta d\xi\right] \\ F_n &= \frac{\pi}{2}Hr^2\sin^2(\alpha) - sr^2\left[\sin(\alpha) - \cos^2(\alpha)\ln\left(\frac{1}{\cos(\alpha)}+\tan(\alpha)\right)\right] \\ \alpha &= \theta = \arctan\sqrt{\frac{h(2r-h)}{r-h}} \end{aligned} \quad (2)$$

Where H is compound surface hardness, s is the shear stress opposite to the sliding direction, α is defined as the angle of a line from the centre of the sphere to the point of first contact with the layer equivalent to the attack angle [20] and ζ, ξ are integration variables. The difference with [22] is the use of the measured depth from the tribometer instead of calculating the depth by adding a modelled elastic deformation to the measured plastic deformation. This choice was made because of the difficulty of establishing a datum on these rough surfaces. Note that this equation assumes bulk properties and is therefore only valid for relatively small depth/coating thickness ratios.

3. Results & discussion

3.1. Nano-indentation as received coatings

The nano-indentation force – displacement curves at 3 mN are presented in Fig. 4. Comparing the indentation depths it can be seen that zinc phosphate (ZnPh, Fig. 4a) has a lower indentation depth than manganese phosphate (MnPh, Fig. 4b). The indentation curves show instability during the indentation phase and large variability in indentation depth. This is most apparent for MnPh. In certain cases the coating failed in the hold phase. The instability and variability indicates brittle material behaviour and subsequent failure of the coating and is confirmed by the absence of elastic recovery.

The processed results in Fig. 5 show the indentation hardness and depth for all applied normal loads. Indeed zinc phosphate is measured as having a higher hardness than manganese phosphate. Multiple indentations reveal a rather large spread in the observed crystal hardness as shown in Fig. 5a. This is attributed to the brittleness combined with the discrete crystals that the coating consists of. Based on the crystal hardness found in literature [1,13] this result is unexpected and can be explained by the following.

First, the approximate point of transition to the substrate hardness from Fig. 5b is used to estimate the coating thickness. The zinc phosphate coating has an average thickness of >6 μm and the manganese phosphate coating >5 μm. This is supported by the coating weight [1].

Second, the area function for the Berkovich indenter is $A = 24.56\,h^2$. This gives for the zinc phosphate 3 mN indentation with h=0.3 μm an A=2.2 μm^2 or an equivalent length (square root of the area) of 1.5 μm. The manganese phosphate 3 mN indentation with h=0.7 μm an A=12 μm^2 gives an equivalent length of 3.5 μm. The lengths are compared to the crystal sizes using the microscopy in Fig. 2 and topography in Fig. 1.

For zinc phosphate the hardness decreases with increasing load which is explained by the roughness and long and narrow needle structure. Under increasing load the contact area will grow beyond the width of the needles reducing the support for the indenter and increasing the measured penetration depth. The results in Fig. 5a support this hypothesis showing decreasing hardness for increasing load and a much lower hardness than expected close to the substrate.

For manganese phosphate the reverse is happening, the hardness increases with load. Potential explanation are that the coating is

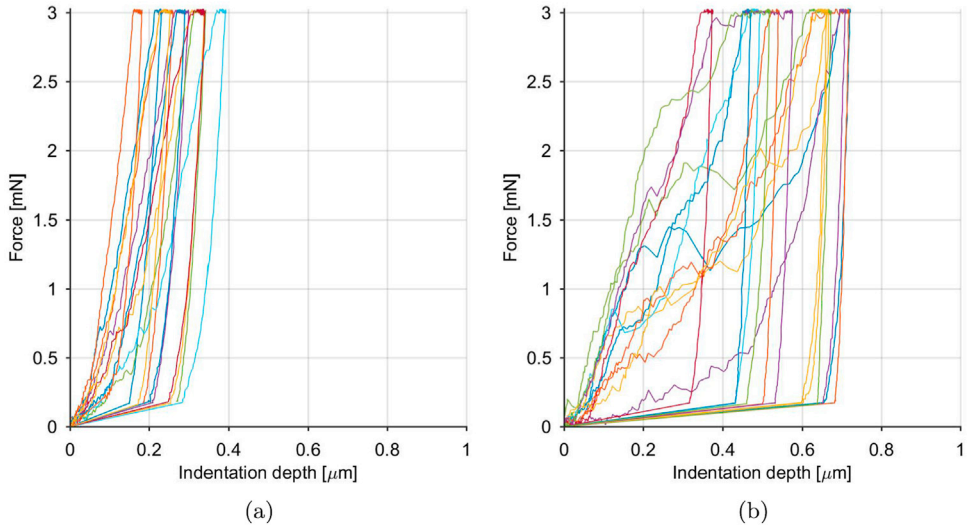

Fig. 4. Nano indentation results for both coating layers. The 3 mN load was applied in 10 s, the hold time was 15 s and unloading was performed in 4 s a) shows the results for zinc phosphate and b) manganese phosphate.

considerably softer and thinner than thought. Or because of the small crystal size the indenter is cleaving the crystals. This is exemplified by the instability during indentation as can be seen in Fig. 4b. As the indentation depth increases more crystals participate in the contact recovering the phosphate bulk hardness. Taking into account the thickness estimation the results in Fig. 5a support the latter hypothesis.

Considering the above, the validity of instrumented hardness measurements and the application of the Oliver & Pharr method [23] for these coatings should be called into question. Therefore the observations are only used qualitatively for the deformation behaviour.

The hypotheses above imply that the effective bulk hardness will be lower than the nano-hardness for zinc phosphate and higher for manganese phosphate. Based on Fig. 1, for zinc phosphate the area covered by the higher needles is about a third. The large needle structure of the zinc phosphate coating will first bear the load. This lowers the effective hardness of the coating. Hence the bulk hardness will depend on two coupled properties: the amount of crystals present on the surface and the size of these crystals. Where the size is dependent on the initial amount of crystal nucleation sites as the growth is restricted by neighbouring crystals [1]. Then the following can be written for the bulk hardness,

$$\begin{aligned} H_c &= \frac{F_n}{A_{indenter}} \\ H_b &= \frac{A_{true}}{A_{total}} H_c \\ \frac{A_{true}}{A_{total}} &= \rho_c A_c \end{aligned} \tag{3}$$

Where H_c is the single crystal hardness as measured with nano-indentation, H_b is the bulk hardness derived from the ensemble of single crystals with area A_c and coverage ρ_c in crystals/square meter defining the true area A_{true} relative to the total area A_{total}.

Applying Eq. (3) to the zinc phosphate example results in a bulk hardness of 600 MPa based on the single crystal hardness of 1800 MPa which is close to the earlier reported value of 50 HV in [14]. For manganese phosphate this is much less of an issue, almost the full area will be in contact owing to the smoothness of the surface. In both cases it means that for high bulk hardness the coating coverage needs to be maximum, advocating a fine and dense coating.

To obtain bulk coating properties from nano-identation of individual crystals the following is proposed. The crystal density and single crystal size can easily be obtained using image recognition software or as is done

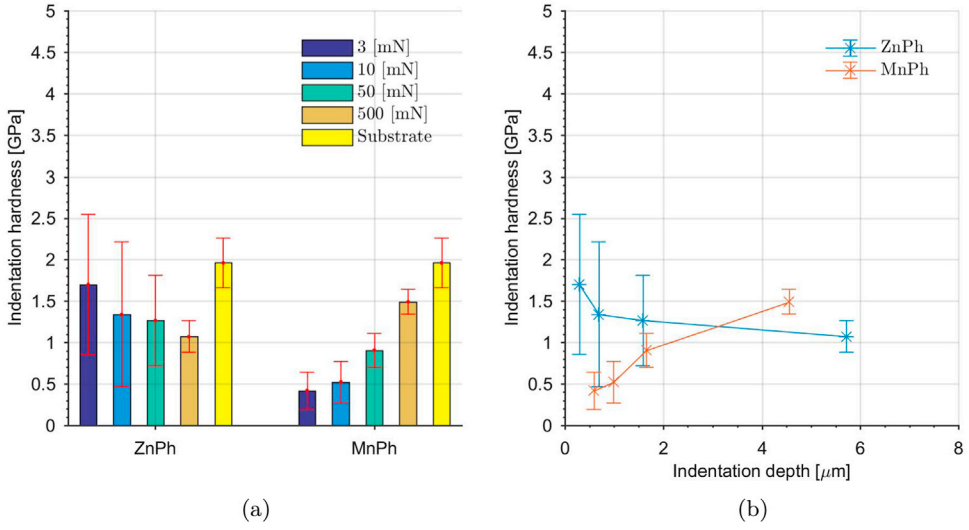

Fig. 5. Statistical results of nano-indentation. a) Gives an overview of the average results for each coating, the error bar indicates the standard deviation. b) Shows the hardness versus indentation depth.

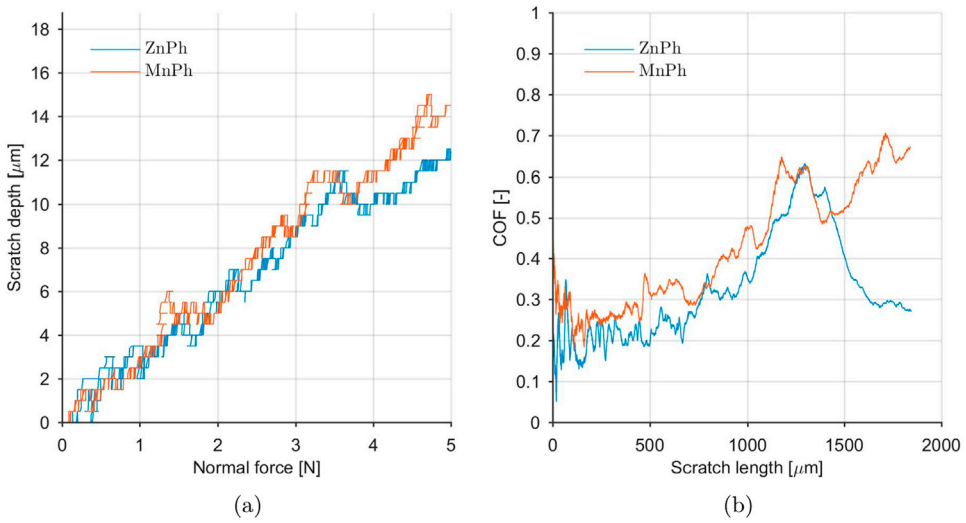

Fig. 6. Results of scratch testing with r=100 μm radius tip. a) Shows depth as function of normal force during sliding. b) Shows the COF versus scratch length.

here the true area can be measured directly from surface topography measurement using a height cut-off filter.

3.2. Scratch hardness and shear strength from ramped load tests

The measured scratch depth versus scratch length and the corresponding COF are depicted in Fig. 6. For both coatings the depth is initially increasing at a similar rate, see Fig. 6a. For zinc phosphate the indenter is reaching the substrate earlier evidenced by the change in penetration rate. Comparing the results in Fig. 6b zinc phosphate has a lower COF than manganese phosphate indicating easier removal of the coating.

Using Eq. (2) the resulting scratch hardness and shear strength are computed and the result is shown in Fig. 7. As with the nano-indentation the crystal density, $\rho_{crystal}$, and associated roughness make it complicated to perform a stable measurement on the specimens. The properties are determined at 10% of the respective coating thickness. The resulting scratch hardness averages around 1.2 GPa and is in agreement with the nano-indentation results of Fig. 5. The shear strength of zinc phosphate averages at 25 MPa which is lower than manganese phosphate at 50 MPa.

The reason for the difference in shear strength is threefold: complete ZnPh needles (see Fig. 8a) are removed, the higher roughness of ZnPh and thus the varying amount of material in front of the indenter and misfit of the ZnPh crystal lattice leading to tensile stresses in the coating. This matches and explains the introductory remarks related to zinc phosphate having lower wear resistance than manganese phosphate.

3.3. Deformation behaviour based on constant load tests

The following qualitative observations are made during the constant load tests and are representative for the full set of experiments. Fig. 8 shows the balls after the 35 N tests. Both zinc Fig. 8a and manganese Fig. 8b phosphate adhere strongly to the counter surface. The transfered layer could not be removed by wiping or ultrasonic cleaning. Note that the angle of attack will be reduced by the presence of the lump of transferred material on the pin similar to the observations of [20]. Fig. 8c and d show the measurement of the average height of the lump on the respective balls. The lumps, disregarding the loose debris, are approximately 10 μm heigh after removal of the sphere.

It is further interesting to note the shape of the transfer layer formed by the transferred phosphate. The shape exactly resembles the contact area during fully plastic sliding, see for instance [24,25] justifying the choice for Eq. (1). Next to that, the debris particles indicate a brittle material. Reinforcing the notion of the coating being crushed by a brittle failure mode. After crushing, the debris is subsequently compacted in the

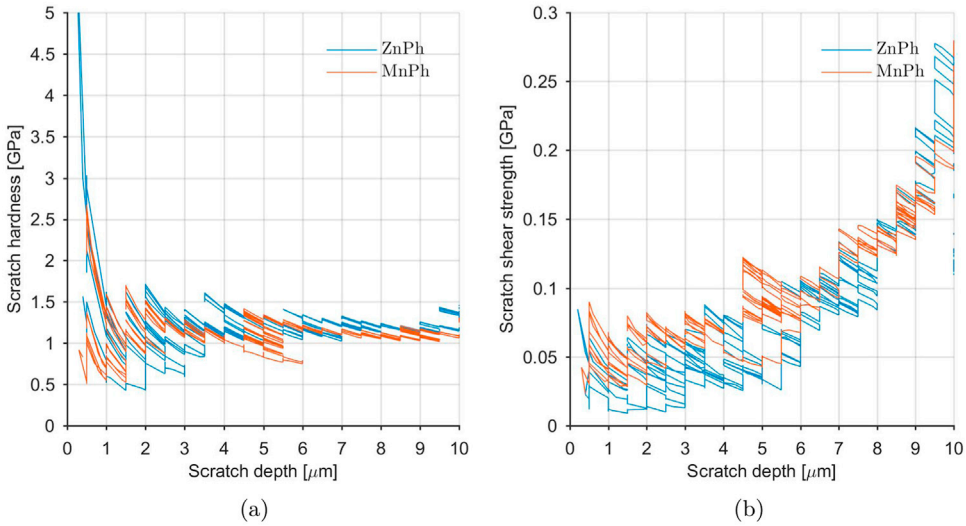

Fig. 7. a) Shows the computed hardness and b) the computed shear strength from the scratch experiments. The results are truncated at 10 μm scratch depth for comparison with Fig. 5. As shown in [22] the hardness converges with increasing depth to the substrate value.

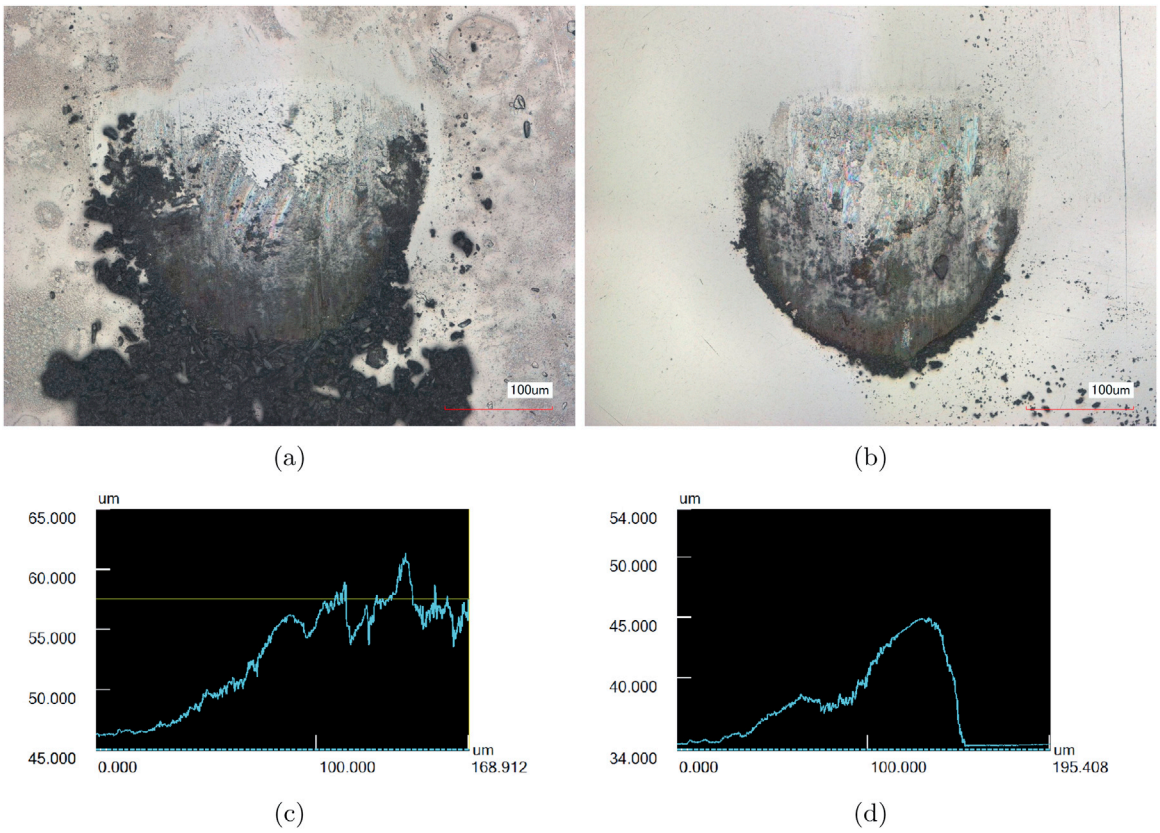

Fig. 8. Comparison between zinc phosphate in a) and manganese phosphate in b) at a normal load of 35 N. Microscopy is taken before cleaning. Images are representative for the complete set. c) Is the measured lump height after subtracting the sphere for a). The same is done for manganese phosphate b) in d).

contact to form the lump. When using a sharp asperity having higher contact angles this is not observed. In that case complete crystals are lifted from the surface comparable to the wedging mode as described by [21].

In Fig. 9 a SEM micrograph is shown of the zinc phosphate transfer layer on the ball. Upon closer inspection brittle fracture lines can be observed in the deposition confirming the earlier observations. Furthermore the layer has the appearance of a densely packed powder which has been polished to a very smooth surface finish. The EDX analysis confirms that the transferred material is indeed consisting of zinc, phosphorus and oxygen.

However, transfer of lumps of phosphate is not always observed. Shown in Fig. 10 are two examples of instances where no transfer occurred, one for each phosphate type. Fig. 10a shows the counter surface after running against zinc phosphate. Fig. 10b shows the counter surface is shown after running against manganese phosphate for which the same observations are made. A silver coloured turning to brown deposition can be observed which is confirmed with EDX to be a thin film

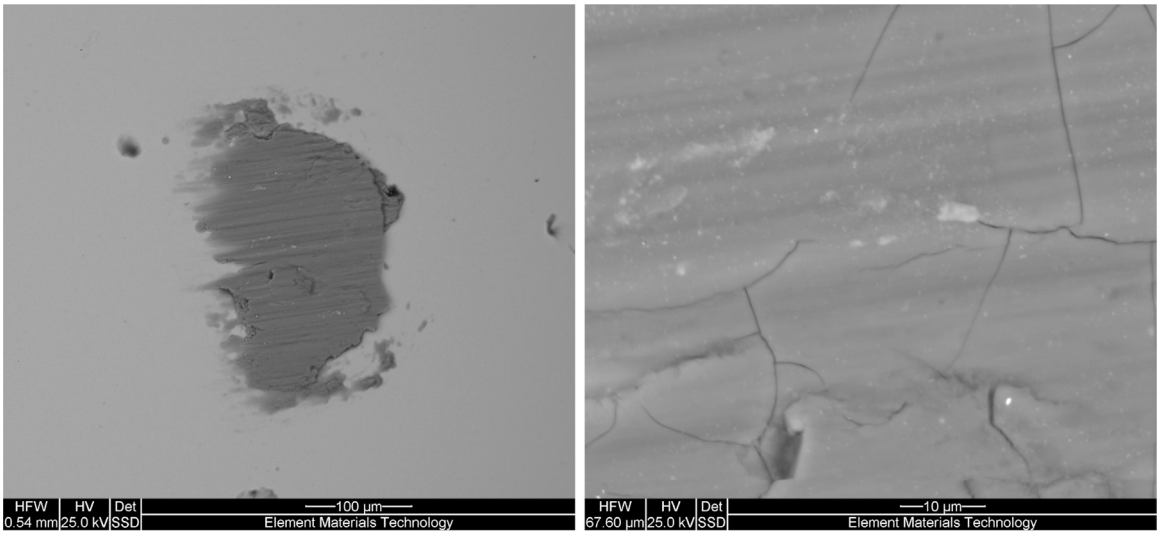

Fig. 9. SEM recording of zinc phosphate transfer layer. Overview on the left, zoom in on the right. The normal force during sliding was 30 N. Clearly visible are what seem to be brittle fractures in the otherwise very smooth transfer film.

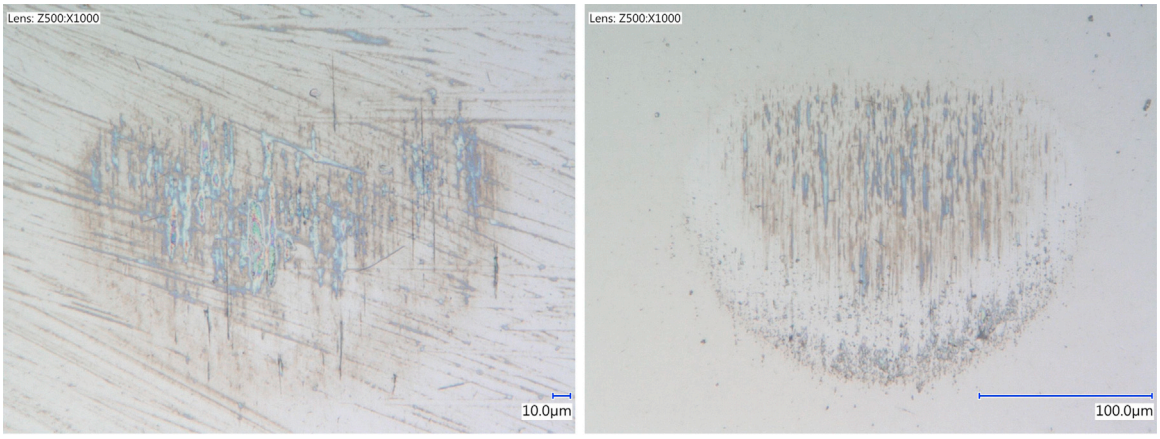

Fig. 10. Overview of the wear scars for dry experiment without transfer to pin. a) Shows zinc phosphate and b) is manganese phosphate. The thin film was confirmed to be zinc or manganese phosphate using EDX.

of zinc or manganese phosphate.

The lack of transfer is explained by the different orientation of the pins with the surface during sliding. Until now all experiments were performed with the direction of grinding of the plate. In this case the wear track described a circular path and thus traversed the ridges of the underlying roughness. Upon traversing material from the pin is deposited in the valleys as described in the previous section.

3.4. Wear tracks

A comparison of two wear tracks is shown in Fig. 11. Fig. 11a and c are zinc phosphate and Fig. 11b and d are manganese phosphate. The lower 2 tracks are after a single scratch experiment, the top two tracks are after 10× repeated unidirectional scratch experiments. Note how initially only the peaks of the zinc phosphate are flattened, after 10× repeated sliding the roughness is filled with the debris which is subsequently compacted and polished. Pile up of removed material is visible at the sides of the wear track. In the manganese phosphate case this is less pronounced due to the smaller crystal size, however, the same mechanism is at play here based on the earlier observations of deposition on the balls.

Further, after formation of a so called glaze layer [1] the wear process enters a second phase of wearing through the formed layer. In this case the layer is thinned until small pieces start to break out according to a

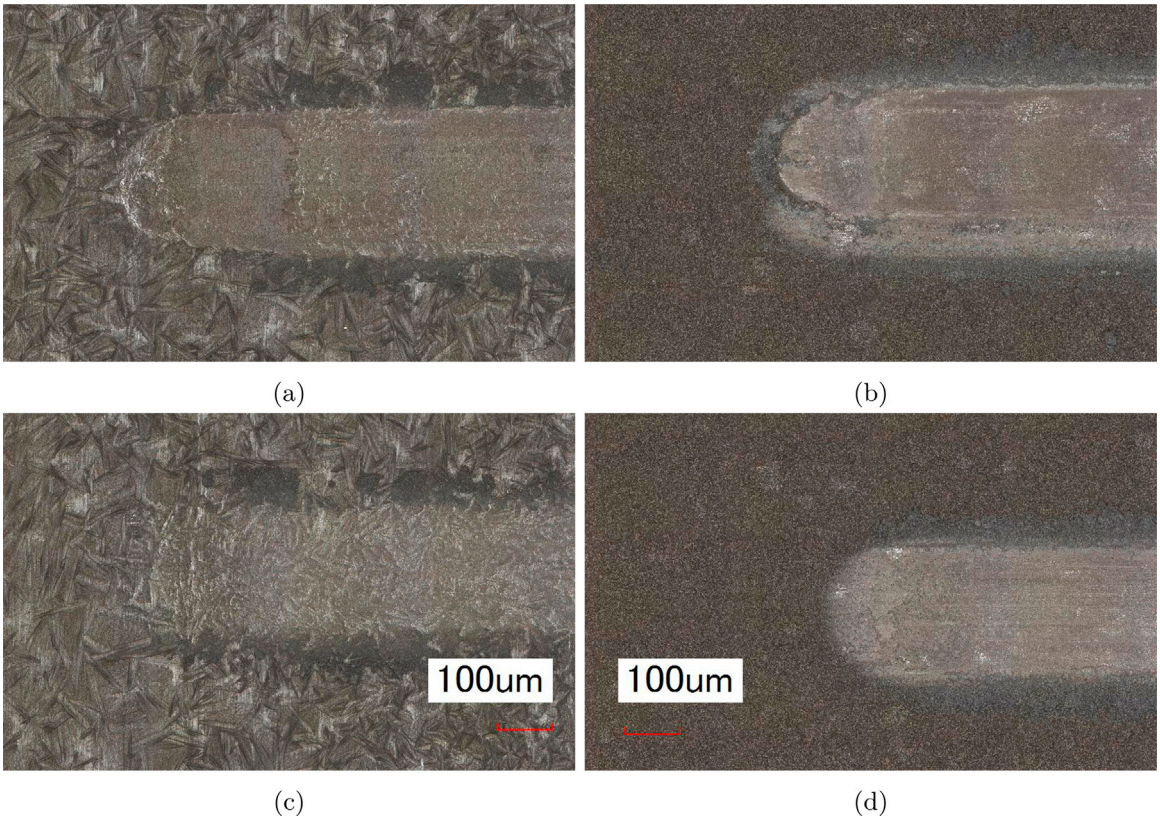

Fig. 11. Comparison of two wear tracks made with a 3 mm ball. Bottom after one pass at 45 N, top after 10 passes at 35 N. Location is at the end of the tracks. a) and c) are zinc phosphate and b) and d) are manganese phosphate. Notice how after one pass the underlying crystal structure is still visible. After 10 passes the layer is compacted and the previously rough crystallographic topology has been polished. Pile up is visible next to the wear tracks.

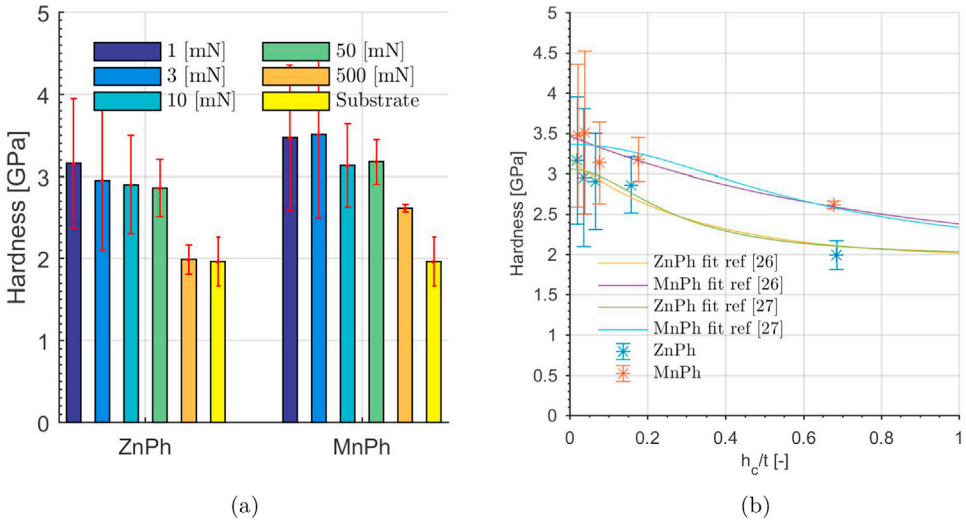

Fig. 12. Statistical results of nano-indentation on the glaze layer. a) Gives an overview of the average results for each coating, the error bar indicates the standard deviation. b) Shows the hardness versus indentation depth compared with a fit using (4) and (5).

mechanism similar to delamination which exposes the underlying substrate. Some of which is starting to occur in Fig. 11a.

3.5. Nano-indentation of formed tribofilm or glaze layer

The topmost wear tracks shown in Fig. 11 were indented with the same loads as previous indentations to investigate the properties of the glaze layer. The results are shown in Fig. 12 and it is observed that the glaze layer possesses a significantly higher surface hardness over a longer depth range compared to the as received coatings. This indicates also a high cohesion between the individual debris particles. Which supports the earlier hypothesis on the formation of a compacted layer of small debris particles under the sliding contact.

A fit of the average indentation results versus depth is made with the following models. The work of [26] states the compound hardness as follows

$$H = H_s + (H_l - H_s)\exp^{-\frac{\beta h_c}{t}}. \quad (4)$$

Where H is the compound indentation hardness, H_s is the substrate hardness, H_l is the layer hardness, β is a constant that depends on the elastic modulus and yield strength of the layer and substrate, h_c is the indentation depth and t is the coating thickness. Korsunsky [27] derived the following relation for the layer to substrate hardness transition

$$H = H_s + \frac{H_l - H_s}{1 + k\left(\frac{h_c}{t}\right)^2}. \quad (5)$$

Where k depends on whether the deformation is plasticity of fracture dominated. Here H_l and β or k are used as fitting parameters. The result is shown in Fig. 12b. The values found from the fitting procedure are shown in Table 3. It shows that the glaze layer exhibits typical behaviour for a hard layer on soft substrate. Care should be taken though because of the large spread on the indentation results.

Note further that even though AISI4130 exhibits plastic strain hardening [28], the hardness increase is entirely attributed to the compaction of the phosphate into a glaze layer. This is supported by the results because at deeper penetration the hardness converges to the "as received" substrate value.

Table 3
Results of the fitting process using the models (4) and (5).

		Model (4), [26]		Model (5), [27]	
Coating	t (μm)	β	H_l (GPa)	k	H_l (GPa)
ZnPh	6	3.1	3.18	14.47	3.06
MnPh	5	1.3	3.47	2.74	3.36

3.6. Implications for the full scale system

Previous investigators [14,15,17,16,1,3] found that zinc phosphate coated systems have a higher wear rate than manganese phosphate. As shown zinc phosphate will in practice exhibit a lower hardness because of a reduced contact area owing to its roughness coming from its dendritic crystal structure. As a consequence the counter surface will penetrate deeper in the coating layer which, combined with its lower shear strength, leads to higher wear.

The mechanism that allows the formation of a glaze layer [1] in phosphated systems was shown to be as follows. The attack angle of the asperity is kept low due to the formation of a lump. Therefore the system remains in the ploughing regime. By keeping the attack angle low, the counter surface compacts and polishes the phosphated surface. Furthermore there is a supply of phosphate to fill gaps in the surface topology which is also subsequently compacted and polished. In contrast, the sharp asperity removed complete crystals from the surface. This advocates the use of phosphates on one surface rubbing against a smooth, hence asperities with low attack angle, counter surface.

4. Conclusions

The mechanical properties and wear characteristics of dry zinc and manganese phosphate coatings were investigated using nano-indentation and a pin-on-disc tribometer. The hardness of the as received coating layers and the formed glaze layer were determined using a Berkovich indenter. Further, the scratch hardness and shear strength of the layers were determined using single asperity scratch tests with a 100 μm and 1500 μm round off asperity.

1. The hardness tests of the as received coatings revealed brittle material behaviour and fracture events. The zinc phosphate nano-hardness was higher compared to manganese phosphate because of the difference in crystal structure.
2. The scratch tests further confirmed the brittle material behaviour. The computed shear strength showed that zinc phosphate has a lower shear strength than manganese phosphate because of complete removal of the needle shaped crystallites.

3. The formation of the glaze layer in phosphate coatings was shown to be related to crushing and compaction of phosphate debris combined with a low attack angle and the formation of a lump on the counter surface. The lump lowered the attack angle keeping the system in the ploughing regime allowing for the counter surface to polish the glaze layer. The lump acts as a reservoir to fill up any gaps in the surface topology leading to a homogeneous and flat glaze layer.
4. The glaze layer has a significantly higher hardness compared to as received coating due to compaction of the worn phosphate crystals in the sliding contact. The layer is brittle owing to the base coating properties as shown by nano-indentation, SEM and the contact area shape. The hardness of the layered system can be satisfactorily described by standard models normally used for metallic layers.

Acknowledgements

The authors are grateful for the permission to publish this work by Shell Global Solutions International BV. Dr. Frank Hollmann and Ralf Schneider of Chemetall GmbH are acknowledged for sharing their knowledge on phosphate conversion coatings and the preparation of the lab specimens.

Appendix A. XRD settings

The crystallographic characterization of the phosphate is performed with a Bruker D8 Discovery HTS diffractometer equipped with a Vantec 2000 detector and a Co2K source. The following measurement parameters were used: Snout: 0.5 [mm], $\theta_1 = 5$, $\theta_2 = 15$, Frames: 3 with a frame width of 28 each, Scan axis: Coupled, Mode: step, Sample oscillation: None, Measurement time/frame: 1200 [s], Slit width: 1.2 [mm] line/0.5 [mm] point. Before the start of the measurements, a reference corundum sample (1776, NIST) is measured to check the alignment of the detector.

References

[1] Rausch W. The phosphating of metals. Metals Park, Ohio, USA; Teddington, Middlesex, England: ASM International; 1990.
[2] Burke D. The sliding friction of bonded solid lubricants [Ph.D. thesis], University of central Lancashire; 2005. URL http://clok.uclan.ac.uk/8690/1/David BurkeMay 05 The Sliding Friction of Bonded Solid Lubricants Degree of Doctor of Philosophy unpublished May05 University of Central Lancashire unknown 320.pdf.
[3] Khaleghi M, Gabe D, Richardson M. Characteristics of manganese phosphate coatings for wear-resistance applications. Wear 1979;55(2):277–87. https://doi.org/10.1016/0043-1648(79)90159-5 [URL ⟨http://linkinghub.elsevier.com/retrieve/pii/0043164879901595⟩ ⟨http://www.sciencedirect.com/science/article/pii/0043164879901595⟩].
[4] Totik Y. The corrosion behaviour of manganese phosphate coatings applied to AISI 4140 steel subjected to different heat treatments. Surf Coat Technol 2006;200(8):2711–7. https://doi.org/10.1016/j.surfcoat.2004.10.004 [URL ⟨http://www.sciencedirect.com/science/article/pii/S0257897204009648⟩ ⟨http://linkinghub.elsevier.com/retrieve/pii/S0257897204009648⟩].
[5] Weng D, Jokiel P, Uebleis A, Boehni H. Corrosion and protection characteristics of zinc and manganese phosphate coatings. Surf Coat Technol 1997;88(1–3):147–56. https://doi.org/10.1016/S0257-8972(96)02860-5 [URL ⟨http://linkinghub.elsevier.com/retrieve/pii/S0257897296028605⟩ arXiv:S0257-8972(96)02860-5].
[6] Ertas A. Experimental investigation of galling resistance in OCTG connections. J Manuf Sci Eng 1992;114(1):100. https://doi.org/10.1115/1.2899745 [URL ⟨http://manufacturingscience.asmedigitalcollection.asme.org/article.aspx?articleid=1447536&resultClick=1⟩].
[7] Pérez-Ràfols F, Larsson R, van Riet EJ, Almqvist A. On the flow through plastically deformed surfaces under unloading: a spectral approach. Proc Inst Mech Eng Part C: J Mech Eng Sci 2017 (095440621769018), http://journals.sagepub.com/doi/10.1177/0954406217690180.
[8] Pérez-Ràfols F, Larsson R, Lundström S, Wall P, Almqvist A. A stochastic two-scale model for pressure-driven flow between rough surfaces. Proc R Soc A: Math Phys Eng Sci 2016;472(2190):20160069. https://doi.org/10.1098/rspa.2016.0069 [URL ⟨http://rspa.royalsocietypublishing.org/lookup/doi/10.1098/rspa.2016.0069⟩].
[9] Pérez-Ràfols F, Larsson R, Almqvist A. Modelling of leakage on metal-to-metal seals. Tribol Int 2016;94:421–7. https://doi.org/10.1016/j.triboint.2015.10.003 [URL ⟨http://linkinghub.elsevier.com/retrieve/pii/S0301679X15004521⟩].
[10] Inose K, Sugino M, Goto K. Influence of grease on high-pressure gas tightness by metal-to-metal seals of premium threaded connections. Tribol Online 2016;11(2):227–34. https://doi.org/10.2474/trol.11.227 [URL ⟨https://www.jstage.jst.go.jp/article/trol/11/2/11_227/_article⟩].
[11] Hill R, Jones J. The crystal structure of hopeite. Am Mineral 1976;61:987–95 [URL ⟨http://www.minsocam.org/ammin/AM61/AM61_987.pdf⟩].
[12] Moore PB, Araki T. Hureaulite, MN52+(H2O)4 [PO3(OH)]2 [PO4]2 – its atomic arrangement. Am Mineral 1973;58(34):302–7.
[13] KozŁowski A. Dry friction of manganese phosphate coatings on steel and cast iron. Electrodepos Surf Treat 1974;2(2):109–22. https://doi.org/10.1016/0300-9416(74)90009-1 [URL ⟨http://linkinghub.elsevier.com/retrieve/pii/0300941674900091⟩].
[14] Kumar A, Bhola S, Majumdar JD. Microstructural characterization and surface properties of zinc phosphated medium carbon low alloy steel. Surf Coat Technol 2012;206(17):3693–9. https://doi.org/10.1016/j.surfcoat.2012.02.052 [URL ⟨http://www.sciencedirect.com/science/article/pii/S0257897212001545⟩ ⟨http://linkinghub.elsevier.com/retrieve/pii/S0257897212001545⟩].
[15] Hivart P, Hauw B, Dubar L, Bricout JPJ. Numerical identification of bulk behavior law of manganese phosphate coatings. Comparison with tribological properties. J Coat Technol 2003;75(942):37–44. https://doi.org/10.1007/BF02730069 [URL ⟨http://link.springer.com/10.1007/BF02730069⟩⟨http://link.springer.com/article/10.1007/BF02730069⟩].
[16] Hivart P, Hauw B, Bricout J, Oudin J. Seizure behaviour of manganese phosphate coatings according to the process conditions. Tribol Int 1997;30(8):561–70. https://doi.org/10.1016/S0301-679X(97)00019-4 [URL ⟨http://www.sciencedirect.com/science/article/pii/S0301679×97000194⟩].
[17] Hivart P, Hauw B, Crampon J, Bricout J. Annealing improvement of tribological properties of manganese phosphate coatings. Wear 1998;219(2):195–204. https://doi.org/10.1016/S0043-1648(98)00211-7 [URL ⟨http://www.sciencedirect.com/science/article/pii/S0043164898002117⟩].
[18] Stewart F, Le H, Williams J, Leech A, Bezensek B, Roberts A. Characterisation of friction and lubrication regimes in premium tubular connections. Tribol Int 2012;53:159–66. https://doi.org/10.1016/j.triboint.2012.04.011 [URL ⟨http://www.sciencedirect.com/science/article/pii/S0301679X12001284⟩].
[19] Bosman R, Hol J, Schipper D. Running-in of metallic surfaces in the boundary lubrication regime. Wear 2011;271(7–8):1134–46. https://doi.org/10.1016/j.wear.2011.05.008 [URL ⟨http://www.sciencedirect.com/science/article/pii/S0043164811003802⟩ ⟨http://linkinghub.elsevier.com/retrieve/pii/S0043164811003802⟩].
[20] de Rooij M, van der Linde G, Schipper D. Modelling material transfer on a single asperity scale. Wear 2013;307(1–2):198–208. https://doi.org/10.1016/j.wear.2013.09.006 [URL ⟨http://linkinghub.elsevier.com/retrieve/pii/S0043164813004870⟩ ⟨http://linkinghub.elsevier.com/retrieve/pii/S0043164813004870⟩].
[21] Hokkirigawa K, Kato K. An experimental and theoretical investigation of ploughing, cutting and wedge formation during abrasive wear. Tribol Int 1988;21(1):51–7. https://doi.org/10.1016/0301-679X(88)90128-4 [URL ⟨http://linkinghub.elsevier.com/retrieve/pii/0301679X88901284⟩].
[22] Tayebi N, Conry TF, Polycarpou AA. Determination of hardness from nanoscratch experiments: corrections for interfacial shear stress and elastic recovery. J Mater Res 2003;18(09):2150–62. https://doi.org/10.1557/JMR.2003.0301 [URL ⟨http://www.mrs.org/jmr_03_0301⟩ ⟨http://www.journals.cambridge.org/abstract_S0884291400064530⟩].
[23] Oliver W, Pharr G. An improved technique for determining hardness and elastic modulus using load and displacement sensing indentation experiments. J Mater Res 1992;7(06):1564–83. https://doi.org/10.1557/JMR.1992.1564 [URL ⟨http://www.journals.cambridge.org/abstract_S0884291400017039⟩].
[24] Masen M, de Rooij M. Abrasive wear between rough surfaces in deep drawing. Wear 2004;256(6):639–46. https://doi.org/10.1016/j.wear.2003.10.006 [URL ⟨http://linkinghub.elsevier.com/retrieve/pii/S0043164803005982⟩ ⟨http://linkinghub.elsevier.com/retrieve/pii/S0043164803005982⟩].
[25] Masen M, de Rooij M, Schipper D. Micro-contact based modelling of abrasive wear. Wear 2005;258(1–4):339–48. https://doi.org/10.1016/j.wear.2004.09.009 [URL ⟨http://linkinghub.elsevier.com/retrieve/pii/S0043164804002510⟩].
[26] Bhattacharya A, Nix W. Analysis of elastic and plastic deformation associated with indentation testing of thin films on substrates. Int J Solids Struct 1988;24(1–2):1287–98. https://doi.org/10.1016/0020-7683(88)90091-1 [URL ⟨http://linkinghub.elsevier.com/retrieve/pii/0020768388900911⟩].
[27] Korsunsky A, McGurk M, Bull S, Page T. On the hardness of coated systems. Surf Coat Technol 1998;99(1–2):171–83. https://doi.org/10.1016/S0257-8972(97)00522-7 [URL ⟨http://linkinghub.elsevier.com/retrieve/pii/S0257897297005227⟩].
[28] Rajan K, Deshpande P, Narasimhan K. Effect of heat treatment of preform on the mechanical properties of flow formed AISI 4130 Steel Tubes-a theoretical and experimental assessment. J Mater Process Technol 2002;125–126:503–11. https://doi.org/10.1016/S0924-0136(02)00305-9 [URL ⟨http://linkinghub.elsevier.com/retrieve/pii/S0924013602003059⟩].